

# Comparison of particle swarm optimization and self-adaptive dynamic differential evolution for the imaging of a periodic conductor

Yu-Ting Cheng, Chien-Ching Chiu\*, Shuo-Peng Chang and Jung-Chin Hsu  
*Electrical Engineering Department, Tamkang University Tamsui, Taiwan*

**Abstract.** The application of two techniques to reconstruct the shape of a two-dimensional periodic perfect conductor from mimic the measurement data is presented. A periodic conducting cylinder of unknown periodic length and shape scatters the incident wave in half-space and the scattered field is recorded outside. After an integral formulation, the microwave imaging is recast as a nonlinear optimization problem; a cost functional is defined by the norm of a difference between the measured scattered electric fields and the calculated scattered fields for an estimated shape of a conductor. Thus, the shape of conductor can be obtained by minimizing the cost function. In order to solve this inverse scattering problem, transverse magnetic (TM) waves are incident upon the objects and two techniques are employed to solve these problems. The first is based on a particle swarm optimization (PSO) and the second is a self-adaptive dynamic differential evolution (SADDE). Both techniques have been tested in the case of simulated mimic the measurement data contaminated by additive white Gaussian noise. Numerical results indicate that the SADDE algorithm is better than the PSO in reconstructed accuracy and convergence speed.

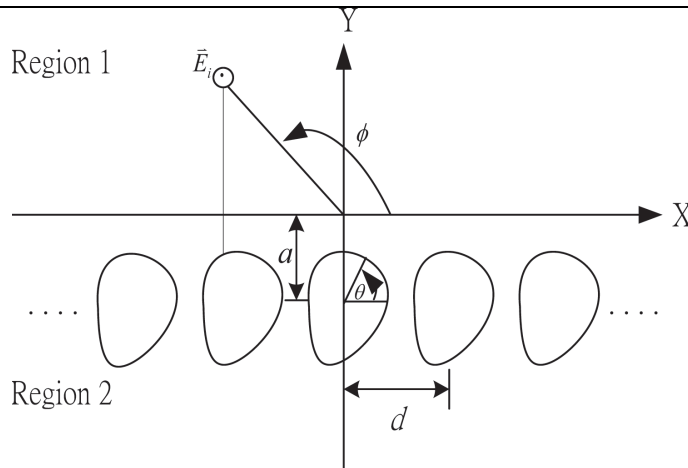
Keywords: Inverse scattering, frequency-domain, self-adaptive dynamic differential evolution, particle swarm optimization

## 1. Introduction

The detection and reconstruction of buried and inaccessible scatterers by inverting microwave electromagnetic data is a research field of considerable interest because of numerous applications in geophysical prospecting, civil engineering, and nondestructive testing. Numerical inverse scattering studies found in the literature are based on either frequency or time domain approaches. However, it is well known that one major difficulty of inverse scattering is its ill-posedness in nature [1].

Another inverse scattering problem is the nonlinearity because it involves the product of two unknowns: the electrical property of object, and the electric field within the object. In general, the nonlinearity of the problem is coped with by applying iterative optimization techniques [2,3]. These algorithms based on stochastic strategies, offer advantages relative to local inversion algorithms including strong search ability, simplicity, robustness, and insensitivity to ill-posedness. In contrast to traditional computation systems, evolutionary computation [4–8] provides a more robust and efficient approach

\*Corresponding author: Chien-Ching Chiu, Electrical Engineering Department, Tamkang University Tamsui, Taiwan.  
E-mail: chiu@ee.tku.edu.tw

Fig. 1. Geometry of the problem in  $(x, y)$  plane.

for solving inverse scattering problems. Particle swarm optimization (PSO) has proven to be a useful method of optimization for difficult and discontinuous multidimensional engineering problems [9,10]. PSO is very efficient at exploring the entire search space. A new method of optimization, Self-Adaptive dynamic differential evolution (SADDE) is able to accomplish the same goal as genetic algorithm (GA) optimization in a new and faster way. Since PSO and SADDE both work with a population of solutions, combining the searching abilities of both methods seems to be a good approach.

Frequency domain inverse scattering by population-based stochastic algorithms are published in the last ten years. Concerning the shape reconstruction of conducting scatterers, the PSO has been investigated whereas the GA has been utilized in the reconstruction of periodic conductor scatterers [11,12]. In this case, the reported results indicate that the PSO is reliable tools for inverse scattering applications. Moreover, it has been shown that both DE and PSO outperform real-coded GA in terms of convergence speed. In recent decade years, some papers have compared different algorithm in inverse scattering [4]. However, to our knowledge, a comparative study about the performances of particle swarm optimization and self-adaptive dynamic differential evolution when applied to inverse scattering problems of a periodic conductor has not yet been investigated.

In this paper, the inverse scattering problem of a periodic perfectly conducting cylinder by transverse magnetic(TM) wave illumination is investigated on the application of both PSO and SADDE. In section II, the solution of the forward scattering problem is presented. In section III and IV, inverse problem and the numerical results of the proposed inverse problem are given, respectively. Section V gives the conclusions.

## 2. Forward problem

Let us consider a periodic cylinder which is partially immersed in a lossy homogeneous half-space, as shown in Fig. 1 Media in regions 1 and 2 are characterized by permittivities and conductivities  $(\epsilon_1, \sigma_1)$  and  $(\epsilon_2, \sigma_2)$  respectively. A perfectly conducting cylinder is illuminated by a TM plane wave. The array is periodic in the  $x$ -direction with a periodic length  $d$  and is uniform in the  $z$ -direction. The cross-section is described in polar coordinates in the  $x, y$  plane by the equation  $\rho = F(\theta)$ . We assume that the time

56 dependence of the field is harmonic with the factor  $e^{j\omega t}$ . Let  $\vec{E}^{inc}$  denote the incident field from region  
 57 1 with incident angle  $\phi$  as shown in Fig. 1. The scattered field,  $\vec{E}_s = E_s \hat{z}$  can be expressed by

$$E_s(x, y) = \int_0^{2\pi} G(x, y; x', y') J(\theta') d\theta' \quad (1)$$

58 Where

$$G(x, y; x', y') = \begin{cases} G_1(x, y; x', y'), & y \leq -a \\ G_2(x, y; x', y'), & y > -a \end{cases} \quad (2)$$

$$59 \quad G_1(x, y; x', y') = \sum_{l=-\infty}^{\infty} \frac{1}{2\pi} \int_{-\infty}^{\infty} \frac{j}{\gamma_1 + \gamma_2} e^{j\gamma_1(y+a)} e^{-j\gamma_2(y'+a)} e^{-j\alpha(x-x'-ld)} d\alpha \quad (3)$$

$$60 \quad G_2(x, y; x', y') = \sum_{l=-\infty}^{\infty} \frac{1}{2\pi} \int_{-\infty}^{\infty} \frac{j}{2\gamma_2} \left( e^{-j\gamma_2|y-y'|} + \frac{\gamma_2 - \gamma_1}{\gamma_2 + \gamma_1} e^{-j\gamma_2(y+2a+y')} \right) e^{-j\alpha(x-x'-ld)} d\alpha \quad (4)$$

$$61 \quad J(\theta) = -j\omega\mu_0 \sqrt{F^2(\theta) + F'^2(\theta)} J_s(\theta) \quad (5)$$

62 With

$$\gamma_q^2 = k_q^2 - \alpha^2, k_q^2 = \omega^2 \mu_0 \varepsilon_q - j\omega_0 \sigma_q, q = 1, 2$$

63 Here  $G(x, y; x', y')$  is the two-dimensional half-space periodic Green's function, and  $J_s(\theta)$  is the in-  
 64 duced surface current density which is proportional to the normal derivative of electric field on the  
 65 conductor surface.  $a$  is buried depth. The boundary condition at the surface of the scatterer states that  
 66 the total tangential electric field must be zero and this yield an integral equation for  $J(\theta)$ :

$$E_i(F(\theta), \theta) = - \int_0^{2\pi} G(x, y, x', y') J(\theta') d\theta' \quad (6)$$

67 For the direct scattering problem, the scattered field  $E_s$  is calculated by assuming that the periodic length  
 68  $d$  and the shape function  $F(\theta)$  of the object is known. This can be achieved by first solving  $J(\theta)$  in  
 69 Eq. (6) and calculating  $E_s$  in Eq. (1). For numerical calculation of the direct problem, the contour is first  
 70 divided into sufficient small segments so that the induced surface current can be considered constant over  
 71 each segment. Then the moment method is used to solve Eqs (6) and (1) with pulse basis function for  
 72 expanding and Dirac delta function for testing. Note that, for numerical implementation of the periodic  
 73 Green's function, we might face some difficulties in calculating this function. In fact, when  $y$  approaches  
 74  $y'$ , the infinite series in Eq. (3), Eq. (4) is very poor convergent. Fortunately, the infinite series may be  
 75 rewritten as a rapidly convergent series plus an asymptotic series which can be summed efficiently. Thus  
 76 the infinite series in the periodic Green's function can be calculated efficiently [11–16].

77 For the inverse problem, assume the approximate center of scatterer, which in fact can be any point  
 78 inside the scatterer, is known. Then the shape function  $F(\theta)$  can be expanded as:

$$F(\theta) = \sum_{n=0}^{N/2} B_n \cos(n\theta) + \sum_{n=1}^{N/2} C_n \sin(n\theta) \quad (7)$$

where  $B_n$  and  $C_n$  are real coefficients to be determined, and  $N + 1$  is the number of unknowns for the shape function. In the inversion procedure, the PSO and SADDE are used to minimize the following objective function:

$$OF = \left\{ \frac{1}{M_t} \sum_{m=1}^{M_t} \left| E_s^{\text{exp}}(\vec{r}_m) - E_s^{\text{cal}}(\vec{r}_m) \right|^2 / |E_s^{\text{exp}}(\vec{r}_m)|^2 \right\}^{1/2} \quad (8)$$

where  $M_t$  is the total number of the mimic measurement data points.  $E_s^{\text{exp}}(\vec{r}_m)$  and  $E_s^{\text{cal}}(\vec{r}_m)$  are the measured and calculated scattered fields, respectively.

### 3. Inverse problem

#### 3.1. Particle swarm optimization

Particle swarm global optimization is a class of derivative-free, population-based and self-adaptive search optimization technique which introduced by Kennedy and Eberhart [3]. Particles are distributed throughout the searching space and their positions and velocities are modified based on social behavior. The social behavior in PSO is a population of particles moving towards the most promising region of the search space. Clerc [17] proposed the constriction factor to adjust the velocity of the particle for obtaining the better convergence; the algorithm was named as constriction factor method.

PSO starts with an initial population of potential solutions that is composed by a group of randomly generated individuals representing shape function of the cylinder. After the initialization step, each particle of population has assigned a randomized velocity and position. Thus, each particle has a position and velocity vector, and moves through the problem space. In each generation, the particle changes its velocity by its best experience, called  $x_{pbest}$ , and that of the best particle in the swarm, called  $x_{gbest}$ . Assume there are  $N_p$  particles in the swarm that is in a search space in  $D$  dimensions, the position and velocity could be determine according to the following equations (constriction factor method):

$$v_{ij}^g = w \cdot v_{ij}^{g-1} + c_1 \cdot \varphi_1 \cdot (X_{pbest_{ij}}^g - x_{ij}^{g-1}) + c_2 \cdot \varphi_2 \cdot (X_{gbest_{ij}}^g - x_{ij}^{g-1}) \quad (9)$$

$$x_{ij}^g = x_{ij}^{g-1} + v_{ij}^g \quad (10)$$

where  $v_{ij}^g$  and  $x_{ij}^g$  are the velocity and position of the  $i$ -th particle in the  $j$ -th dimension at  $g$ -th generation,  $\varphi_1$  and  $\varphi_2$  are both the random number between 0 and 1,  $c_1$  and  $c_2$  are learning coefficients and  $w$  is the inertial weighting factor that can avoid the particle trapped into the local minimized solution.

It should be noted that the shape function used to describe the shape of the cylinder will be determined by the PSO scheme. The flowchart of the PSO is shown in Fig. 2. PSO goes through five procedures as follows:

1. Initialize a starting population: Randomly generate a swarm of particles.
2. Calculate  $E$  fields.
3. Evaluate the population using objective function: The PSO algorithm evaluates the objective function Eq. (8) for each individual in the population.
4. Find  $x_{pbest}$  and  $x_{gbest}$ .
5. Update the velocity and position.

Stop the process and print the best individual if the termination criterion is satisfied, else go to step II.

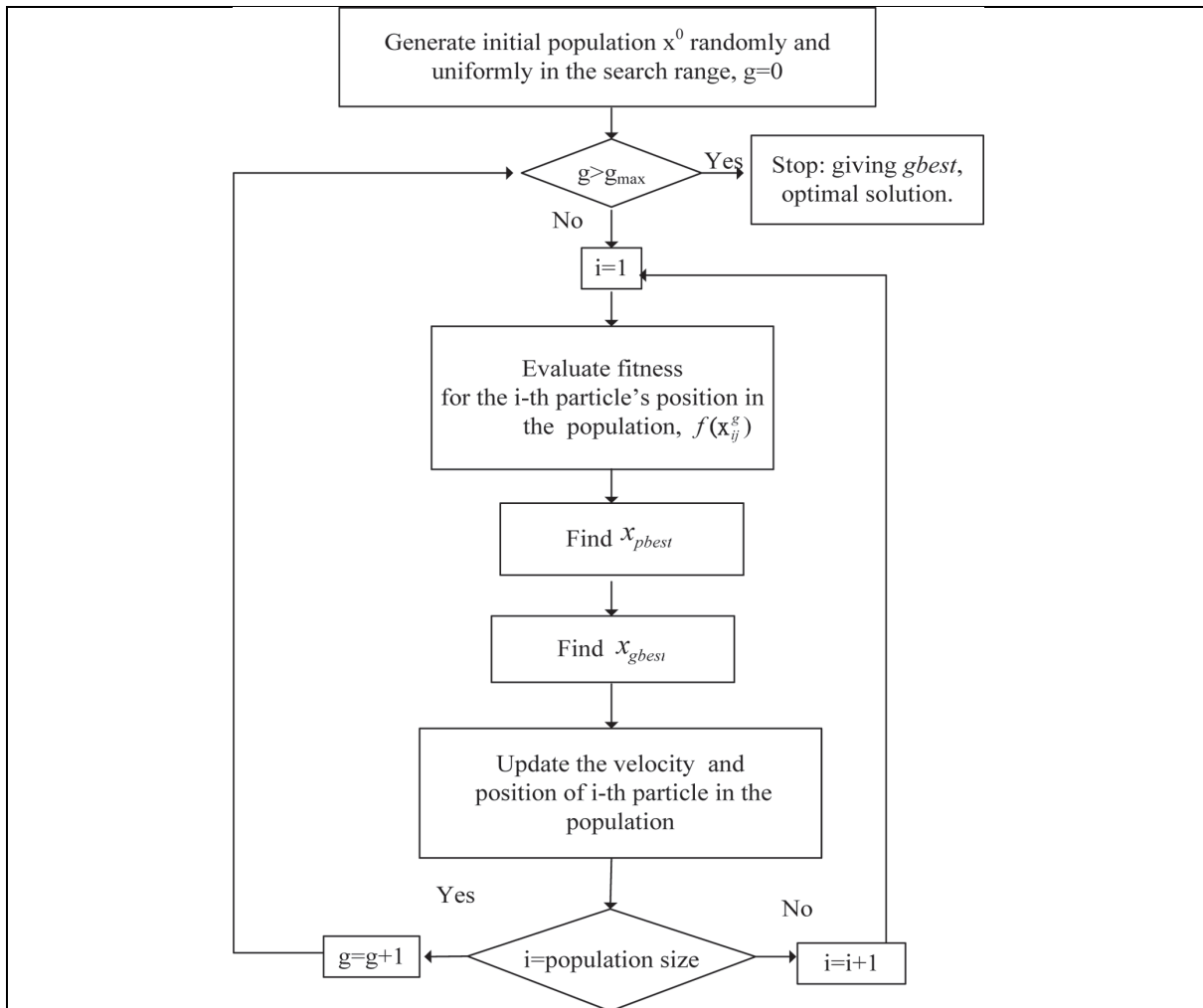


Fig. 2. Flowchart for the particle swarm optimization (PSO).

### 113 3.2. Self-Adaptive Dynamic Differential Evolution (SADDE)

114 The SADDE are based on DDE scheme. The SADDE algorithm starts with an initial population of  
 115 potential solutions that is composed by a group of randomly generated individuals which represents  
 116 periodic length and the shape function of the cylinders. The flowchart of the SADDE algorithm is shown  
 117 in Fig. 3. SADDE algorithm goes through six procedures as follows:

- 118 1. Initialize a starting population: Individuals in SADDE algorithm represent a set of  $D$ -dimensional  
 119 vectors in the parameter space for the problem,  $\{X_i : i = 1, 2, \dots, Np\}$ , where  $D$  is the number  
 120 of parameters to be optimized and  $Np$  is the population size.
- 121 2. Evaluate the population using cost function: After initialization, SADDE algorithm evaluates the  
 122 objective function Eq. (8) for each individual in the population.
- 123 3. Perform mutation operation to generate trial vectors: The mutation operation of SADDE algorithm  
 124 is performed by arithmetical combination of individuals. For each parameter vector  $X_i$  of the parent

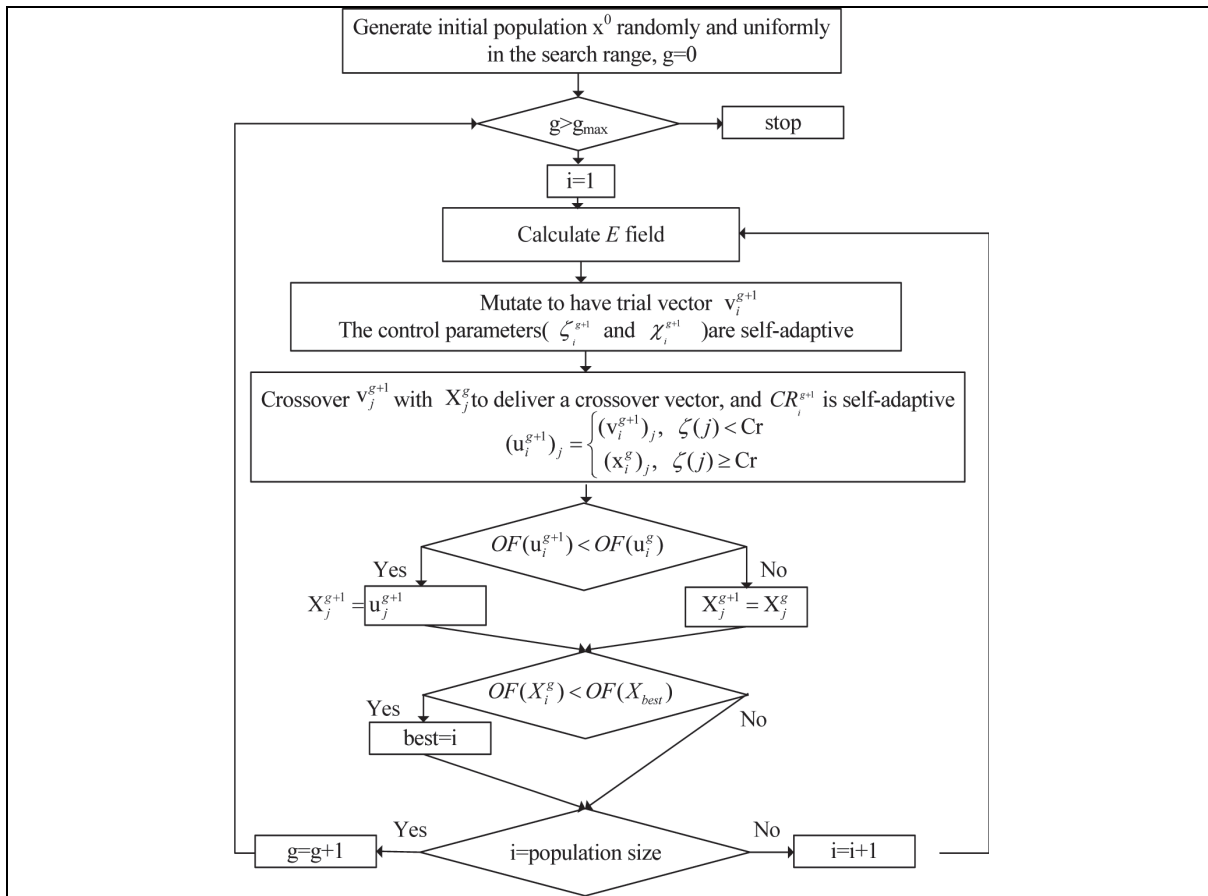


Fig. 3. Flowchart for the self-adaptive dynamic differential evolution (SADDE).

125 generation, a trial vector  $V_i$  is generated according to the following equation:

$$126 \quad (V_i^{g+1})_j = (X_i^g)_j + \xi \cdot [(X_{best}^g)_j - (X_i^g)_j] + \chi \cdot [(X_m^g)_j - (X_n^g)_j],$$

$$127 \quad m, n \in [0, N_p - 1], m \neq n \quad (11)$$

128 where  $\xi$  and  $\chi$  are the scaling factors associated with the vector differences  $(X_{best}^g - X_i^g)$  and  $(X_m^g - X_n^g)$ , respectively. The disturbance vector  $V$  due to the mutation mechanism consists of  
 129 parameter vector  $X_i^g$ , the best particle  $X_{best}^g$  and two randomly selected vectors. Note that  $\xi$  and  $\chi$  are adjusted automatically.

130 In SADDE, The basic idea is to have the control parameters evolve through generations. New  
 131 vectors are generated by using the evolved values of the control parameters. These new vectors are  
 132 more likely to survive and produce offspring during the selection procedure. In turn, the survived  
 133 vectors carry the improved values of the control parameters to the next generation. Therefore,  
 134 the control parameters are self-adjusted in every generation for each individual according to the  
 135 following scheme:

$$\xi_i^{g+1} = \begin{cases} \xi_l + rand_1 * \xi_u, & \text{if } rand_2 < 0.1 \\ \xi_i^g, & \text{otherwise} \end{cases} \quad (12)$$

$$\chi_i^{g+1} = \begin{cases} \chi_l + rand_3 * \chi_u, & \text{if } rand_4 < 0.1 \\ \chi_i^g, & \text{otherwise} \end{cases} \quad (13)$$

where  $rand1$ ,  $rand2$ ,  $rand3$  and  $rand4$  are random numbers with the values uniformly distributed between 0 and 1.  $\xi_l$ ,  $\xi_u$ ,  $\chi_l$  and  $\chi_u$  are the lower and the upper limits of  $\xi$  and  $\chi$ , respectively. Both  $\xi_l$  and  $\chi_l$  are set to 0.1 and both  $\xi_u$  and  $\chi_u$  are set to 0.9 [18,19].

4. Perform crossover operation with probability of crossover  $Cr$  to deliver crossover vectors: The crossover operation of SADDE algorithm is performed to increase the diversity of the parameter vectors. This operation is similar to the crossover process in GAs. However, the crossover operation of SADDE algorithm just allows to deliver the crossover vector  $u_i$  by mixing component of the current vector  $X_i^g$  and the trial vector  $V_i$ . It can be expressed as:

$$(u_i^{g+1})_j = \begin{cases} (V_i^{g+1})_j, & \zeta(j) < Cr \\ (X_i^g)_j, & \zeta(j) \geq Cr \end{cases} \quad (14)$$

$$Cr_i^{g+1} = \begin{cases} rand_5, & \text{if } rand_6 < 0.1 \\ Cr_i^g, & \text{otherwise} \end{cases} \quad (15)$$

where  $Cr$  is the probability of crossover,  $Cr \in (0, 1)$ .  $rand5$  and  $rand6$  are random numbers with the values uniformly distributed between 0 and 1.  $\zeta(j)$  is the random number generated uniformly between 0 and 1.

5. Perform selection operation to produce offspring: Selection operation is conducted by comparing the parent vector  $X_i^g$  with the crossover vectors  $u_i^{g+1}$ . The vector with smaller cost function value is selected as a member of the next generation. Explicitly, the selection operation for the minimization problem is given by:

$$X_i^{g+1} = \begin{cases} u_i^{g+1}, & \text{if } OF(u_i^{g+1}) < OF(X_i^g) \\ X_i^g, & \text{otherwise} \end{cases} \quad (16)$$

The SADDE algorithm is carried out in a dynamic way: each parent individual will be replaced by his offspring if the offspring has a better cost function value than its parent individual does.

6. Stop the process and obtain the best individual if the termination criterion is satisfied, else go to step 2.

The algorithm of SADDE is a self-adaptive version of DDE, which is processed of self-adaptability and the ability of approaching the "Best". Based on the self-adaptive concept, the parameters  $\xi$ ,  $\chi$  and  $Cr$  adjust automatically while the time complexity does not increase.

#### 4. Numerical results

We illustrate the performance of the proposed inversion algorithm and its sensitivity to random noise in the scattered field. Let us consider a perfectly conducting cylinder buried in a lossless half-space ( $\sigma_1 = \sigma_2 = 0$ ). The permittivity in each region is characterized by  $\varepsilon_1 = \varepsilon_0$  and  $\varepsilon_2 = 2.56\varepsilon_0$  respectively. The frequency of the incident wave is chosen to be 1 GHz with incident angles  $\phi$  equal to  $45^\circ$ ,  $90^\circ$  and  $135^\circ$ , respectively. The wavelength  $\lambda_0$  is 0.1 m. For each incident wave, 18 measurements are made at the points equally separated on a semi-circle with the radius of 2.1 m in region 1. There are 54 measurement points in each simulation. We set the total number of generation to be 500 (i.e.,  $g_{\max} = 500$ ),  $c_1$  and  $c_2$  to be 1.3 and 2.8 respectively. The population size is chosen as 35. Number of unknowns is set to be 8 (i.e.,  $N + 2 = 8$ ), In other words, seven unknowns for the shape function  $F(\theta)$  and one unknowns for

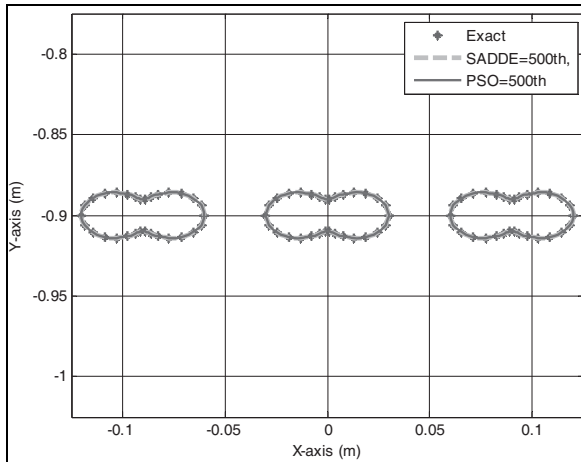


Fig. 4. The reconstructed shape of the cylinder for example 1.

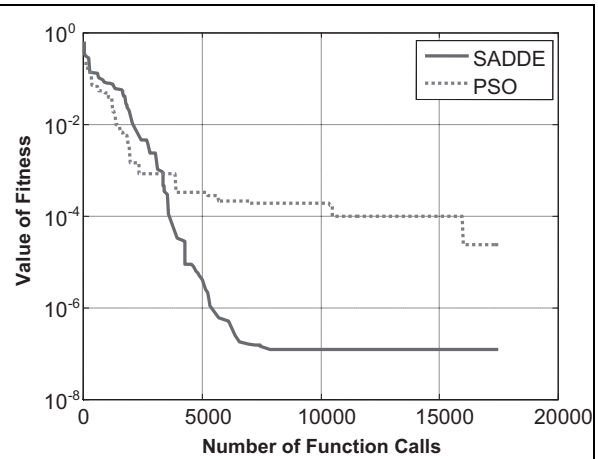


Fig. 5. The value of fitness versus the number of function calls for example 1.

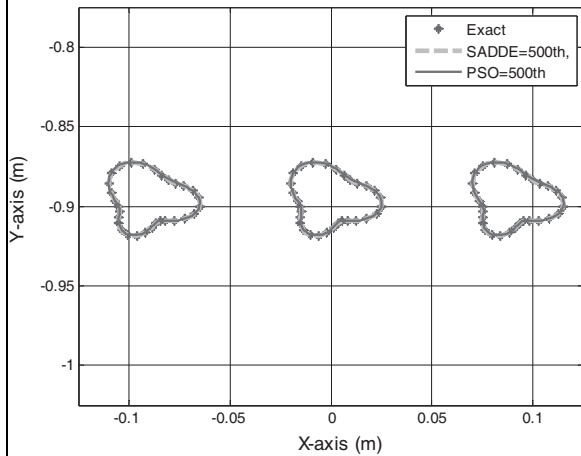


Fig. 6. The reconstructed shape of the cylinder for example 2.

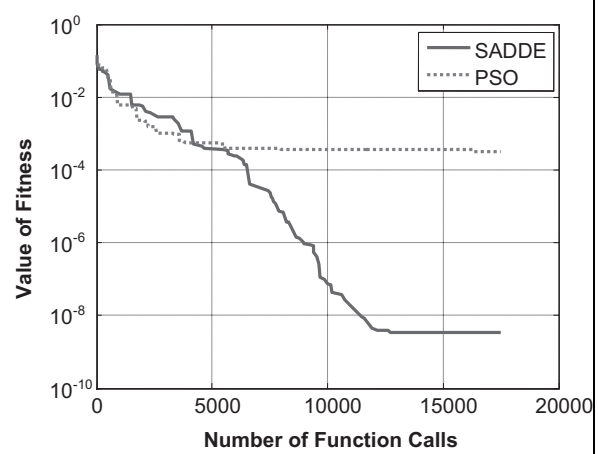


Fig. 7. The value of fitness versus the number of function calls for example 2.

169 period length. The search range for the unknown coefficient of the shape function is chosen to be from  
 170 0 to 0.1. The search range for the unknown periodic length is chosen from 0.05 to 0.1. Our purpose is to  
 171 reconstruct the shape of the object by using the scattered field at different incident angles.

172 Three examples are investigated for the inverse scattering of the proposed structure by using the PSO  
 173 and SADDE. In the first example, the shape function is chosen to be  $F(\theta) = (0.02 + 0.01 \cos 2\theta)$  m. The  
 174 reconstructed shape function of PSO and SADDE for the best population member is plotted in Fig. 4  
 175 and the value of fitness versus the number of function calls for example 1 is shown in Fig. 5. The number  
 176 of function calls is the number of the calculation of direct problem. The total number of function calls  
 177 is the total generations multiply by population size. The reconstructed shape error by PSO and SADDE  
 178 are 0.4% and 0.1%, respectively. It is clear that the reconstructed result is good.

179 In the second example, the shape function is chosen to be  $F(\theta) = (0.02 + 0.005 \cos 3\theta + 0.005 \sin \theta)$   
 180 m. This example shows that the proposed scheme can reconstruct more complicated scatterer whose



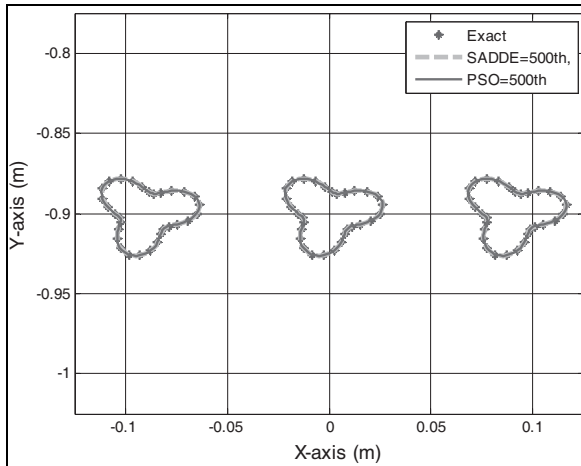


Fig. 8. The reconstructed shape of the cylinder for example 3.

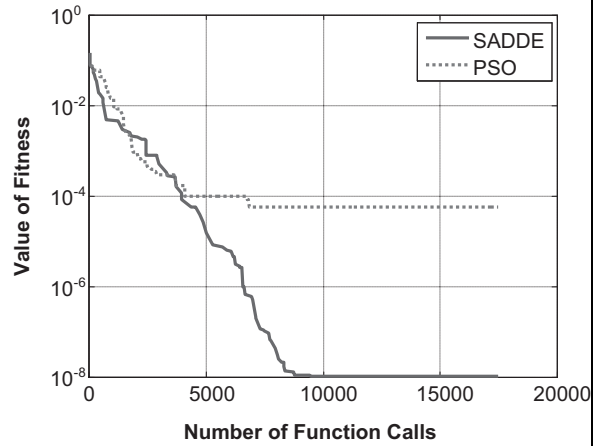


Fig. 9. The value of fitness versus the number of function calls for example 3.

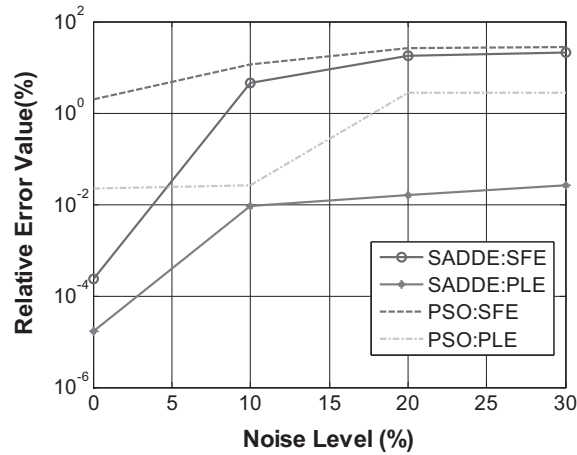


Fig. 10. Shape function error and periodic length error as functions of noise level by PSO and SADDE.

181 shape function has three concavities. The reconstructed shape function for the best population member  
 182 is plotted in Fig. 6 and the value of fitness versus the number of function calls for example 2 is shown in  
 183 Fig. 7. The reconstructed shape error by PSO and SADDE are 1.33% and 0.62%, respectively. There is  
 184 a small discrepancy in the bottom of the shape since TM waves are incident from the top of the shape.

185 In the third example, the shape function is chosen to be  $F(\theta) = (0.02 + 0.005 \cos 3\theta + 0.005 \sin 3\theta)m$ .  
 186 The reconstructed shape function for the best population member is plotted in Fig. 8 and the value of  
 187 fitness versus the number of function calls for example 3 is shown in Fig. 9. The reconstructed shape  
 188 error by PSO and SADDE are 2.03% and 0.6%, respectively. It is seen that the error comes from the  
 189 bottom of the shape, but we still can obtain good results by PSO algorithm and SADDE.

190 From the three example, it is observed that PSO converges faster when the number of function calls  
 191 are less than 5000. However, SADDE can get more accurate results when the number of function calls  
 192 became large. As a result, SADDE are better than PSO for the complex objects. To investigate the effects  
 193 of noise, we add to each complex scattered field a quantity  $b + cj$ , where  $b$  and  $c$  are independent random

194 numbers having a uniform distribution over 0 to the noise level times the R.M.S value of the scattered  
 195 field. Normalized standard deviations of 10%, 20% and 30%, respectively, are used in the simulations.  
 196 Figure 10 shows the reconstructed results under the condition that the scattered E fields to mimic the  
 197 measurement data contaminated by the noise. The discrepancy of shape function of the reconstructed  
 198 shape is shown in Fig. 10. Here *PLE* and *SFE*, which are called periodic length error and shape function  
 199 discrepancies, respectively, are defined as

$$PLE = \frac{|d^{cal} - d|}{d} \quad (17)$$

$$SFE = \left\{ \frac{1}{N'} \sum_{i=1}^{N'} [F^{cal}(\theta_i) - F(\theta_i)]^2 / F^2(\theta_i) \right\}^{1/2} \quad (18)$$

201 where  $N'$  is set to 100. Quantities *PLE* and *SFE* provide measures of how well  $d^{cal}$  approximates  $d$   
 202 and  $F^{cal}(\theta)$  approximates  $F(\theta)$ , respectively. It could be observed that good reconstruction has been  
 203 obtained for shape of the perfectly conducting cylinder when the relative noise level is below 10%.

## 204 5. Conclusion

205 The problems of the periodic length and shape reconstruction of periodic conducting cylinder are  
 206 investigated. Based on the boundary condition and the measured scattered field, we have derived a set  
 207 of nonlinear integral equations and reformulated the imaging problem into an optimization one which  
 208 solved by applying SADDE and PSO techniques.

209 The objective function of both PSO and SADDE is to minimize the discrepancy between measured  
 210 and estimated scattered field data. Numerical results show that SADDE outperforms the PSO in terms of  
 211 accuracy and convergence speed, when the same number of iterations is applied, since SADDE realizes  
 212 the ideas of approaching the “Self-Adaptive”. SADDE algorithm can result in accurate reconstruction  
 213 even when the effects of noise are included under the condition of noise level less than  $10^{-2}$ .

## 214 References

- 215 [1] P.C. Sabatier, Theoretical Considerations For Inverse Scattering, *Radio Science* **18** (Jan. 1983), 629–631.  
 216 [2] R. Storn and K. Price, Differential Evolution – a Simple and Efficient Adaptive Scheme for Global Optimization over  
 217 Continuous Spaces, Technical Report TR-95-012, International Computer Science Institute, Berkeley, 1995.  
 218 [3] J. Kennedy and R.C. Eberhart, Particle Swarm Optimization, *Proceedings of the IEEE International Conference on*  
 219 *Neural Network*, 1995, pp. 1942–1948.  
 220 [4] I.T. Rekanos, Shape Reconstruction of a Perfectly Conducting Scatterer Using Differential Evolution and Particle Swarm  
 221 Optimization, *IEEE Transactions on Geoscience and Remote Sensing* **46**(7) (2008), 1967–1974.  
 222 [5] A. Semnani and M. Kamyab, An Enhanced Method for Inverse Scattering Problems Using Fourier Series Expansion in  
 223 Conjunction with FDTD and PSO, *Progress In Electromagnetic Research* **PIER 76** (2007), 45–64.  
 224 [6] A. Semnani, M. Kamyab and I.T. Rekanos, Reconstruction of One-Dimensional Dielectric Scatterers Using Differential  
 225 Evolution and Particle Swarm Optimization, *IEEE Geoscience and Remote Sensing Letters* **6**(4) (Oct. 2009), 671–675.  
 226 [7] K.A. Michalski, Electromagnetic Imaging of Circular-Cylindrical Conductors and Tunnels Using A Differential Evolu-  
 227 tion Algorithm, *Microwave and Optical Technology Letters* **27**(5) (Dec. 2000), 330–334.  
 228 [8] W. Chien, C.H. Huang, C.C. Chiu and C.L. Li, Image Reconstruction for 2D Homogeneous Dielectric Cylinder Using  
 229 FDTD Method and SSGA, *International Journal of Applied Electromagnetics and Mechanics* **32**(2) (Feb. 2010), 111–  
 230 123.

- 231 [9] S. Zhang, S.-X. Gong, Y. Guan, P.-F. Zhang and Q. Gong, A Novel IGA-EDSPSO Hybrid Algorithm for the Synthesis  
232 of Sparse Arrays, *Progress In Electromagnetic Research* **PIER 89** (2009), 121–134.
- 233 [10] W.-T. Wang, S.-X. Gong, Y.-J. Zhang, F.-T. Zha, J. Ling and T. Wan, Low RCS Dipole Array Synthesis Based on MoM-  
234 PSO Hybrid Algorithm, *Progress In Electromagnetic Research*, PIER 94, 2009, pp. 119–132.
- 235 [11] W. Chien, C.H. Huang and C.C Chiu, Cubic-Spline expansion for a Two-Dimensional Periodic Conductor in Free Space,  
236 *International Journal of Applied Electromagnetics and Mechanics* **24**(1–2) (Nov. 2006).
- 237 [12] C.C. Chiu and C.S. Ho, Image Reconstruction of a Two-Dimensional Periodic Conductor by the Genetic Algorithm,  
238 *Journal of Electromagnetic Waves and Applications* **15**(9) (Sept. 2001), 1175–1188.
- 239 [13] R.E. Jorgenson and R. Mittra, Efficient calculation of free-space periodic Green's function, *IEEE Trans. Antenna Prop-*  
240 *agat* **38** (May 1990), 633–642.
- 241 [14] G.S. Wallinga, E.J. Rothwell, K.M. Chen and D.P. Nyquist, Efficient computation of the two-dimensional periodic  
242 Green's function, *IEEE Tran. Antenna Propagat* **47** (May 1999), 895–897.
- 243 [15] S. Boutami and M. Fall, Calculation of Free-Space Periodic Green's Function Using Equivalent Finite Array, *IEEE*  
244 *Transactions on Antennas and Propagation* **60** (2012), 4725–4731.
- 245 [16] D. Van Orden and V. Lomakin, Rapidly Convergent Representations for Periodic Green's Functions of a Linear Array in  
246 Layered Media, *IEEE Transactions on Antennas and Propagation* **60**(2) (2012), 870–879.
- 247 [17] M. Clerc, The swarm and the queen: Towards a deterministic and adaptive particle swarm optimization, *Proceedings of*  
248 *Congress on Evolutionary Computation*, Washington, DC, 1999, pp. 1951–1957.
- 249 [18] J. Brest, S. Greiner, B. Boskovic, M. Mernik and V. Zumer, Self-adapting control parameters in differential evolution:  
250 comparative study on numerical benchmark problems, *IEEE Transactions on Evolutionary Computation* **10**(6) (Dec.  
251 2006), 646–657.
- 252 [19] S.K. Goudos, K. Siakavara, T. Samaras, E.E. Vafiadis and J.N. Sahalos, Self-Adaptive Differential Evolution Applied to  
253 Real-Valued Antenna and Microwave Design Problems, *IEEE Transactions on Antennas and Propagation* **59**(4) (Apr.  
254 2011), 1286–1298.
-